



Exploring neutrino–nucleus interactions in the GeV regime using MINERvA

X.-G. Lu^{1,a} , Z. Ahmad Dar^{2,3}, F. Akbar³, D. A. Andrade⁴, M. V. Ascencio⁵, G. D. Barr¹, A. Bashyal⁶, L. Bellantoni⁷, A. Bercellie⁸, M. Betancourt⁷, A. Bodek⁸, J. L. Bonilla⁴, H. Budd⁸, G. Caceres⁹, T. Cai⁸, M. F. Carneiro^{6,9,23}, H. da Motta⁹, G. A. Díaz⁸, J. Felix⁴, L. Fields⁷, A. Filkins², R. Fine^{8,24}, A. M. Gago⁵, H. Gallagher¹⁰, S. M. Gilligan⁶, R. Gran¹¹, D. A. Harris^{7,12}, S. Henry⁸, D. Jena⁷, S. Jena¹³, J. Kleykamp⁸, A. Klustová¹⁴, M. Kordosky², D. Last¹⁵, A. Lozano⁹, E. Maher^{16,25}, S. Manly⁸, W. A. Mann¹⁰, C. Mauger¹⁵, K. S. McFarland⁸, A. M. McGowan⁸, B. Messerly^{17,26}, J. Miller¹⁸, J. G. Morfín⁷, D. Naples¹⁷, J. K. Nelson², C. Nguyen¹⁹, A. Olivier⁸, V. Paolone¹⁷, G. N. Perdue^{7,8}, K.-J. Plows¹, M. A. Ramírez^{4,15}, R. D. Ransome²⁰, H. Ray¹⁹, P. A. Rodrigues^{1,8,21}, D. Ruterbories⁸, H. Schellman⁶, C. J. Solano Salinas²², H. Su¹⁷, M. Sultana⁸, V. S. Syrotenko¹⁰, E. Valencia^{2,4}, A. V. Waldron¹⁴, D. Wark¹, A. Weber¹, K. Yang¹, and L. Zazueta²
(The MINERvA Collaboration)

¹ Department of Physics, University of Oxford, Oxford OX1 3PJ, UK

² Department of Physics, William & Mary, Williamsburg, VA 23187, USA

³ AMU Campus, Aligarh, Uttar Pradesh 202001, India

⁴ Campus León y Campus Guanajuato, Universidad de Guanajuato, Lascrain de Retana No. 5, Colonia Centro, 36000 Guanajuato, Guanajuato, Mexico

⁵ Sección Física, Departamento de Ciencias, Pontificia Universidad Católica del Perú, Apartado 1761, Lima, Peru

⁶ Department of Physics, Oregon State University, Corvallis, OR 97331, USA

⁷ Fermi National Accelerator Laboratory, Batavia, IL 60510, USA

⁸ University of Rochester, Rochester, NY 14627, USA

⁹ Centro Brasileiro de Pesquisas Físicas, Rua Dr. Xavier Sigaud 150, Urca, Rio de Janeiro, Rio de Janeiro 22290-180, Brazil

¹⁰ Physics Department, Tufts University, Medford, MA 02155, USA

¹¹ Department of Physics, University of Minnesota, Duluth, Duluth, MN 55812, USA

¹² Department of Physics and Astronomy, York University, Toronto, ON M3J 1P3, Canada

¹³ Department of Physical Sciences, IISER Mohali, Knowledge City, SAS Nagar, Mohali, Punjab 140306, India

¹⁴ The Blackett Laboratory, Imperial College London, London SW7 2BW, UK

¹⁵ Department of Physics and Astronomy, University of Pennsylvania, Philadelphia, PA 19104, USA

¹⁶ Massachusetts College of Liberal Arts, 375 Church Street, North Adams, MA 01247, USA

¹⁷ Department of Physics and Astronomy, University of Pittsburgh, Pittsburgh, PA 15260, USA

¹⁸ Departamento de Física, Universidad Técnica Federico Santa María, Avenida España 1680, Casilla 110-V, Valparaíso, Chile

¹⁹ Department of Physics, University of Florida, Gainesville, FL 32611, USA

²⁰ Rutgers, The State University of New Jersey, Piscataway, NJ 08854, USA

²¹ University of Mississippi, Oxford, MS 38677, USA

²² Facultad de Ciencias, Universidad Nacional de Ingeniería, Apartado 31139, Lima, Peru

²³ Present address: Brookhaven National Laboratory, Upton, USA

²⁴ Present address: Los Alamos National Laboratory, Los Alamos, USA

²⁵ Department of Physics, Chennai, India

²⁶ Present address: University of Minnesota, Minneapolis, USA

Received 4 July 2021 / Accepted 23 September 2021 / Published online 3 November 2021

© The Author(s) 2021

Abstract With the advance of particle accelerator and detector technologies, the neutrino physics landscape is rapidly expanding. As neutrino oscillation experiments enter the intensity and precision frontiers, neutrino–nucleus interaction measurements are providing crucial input. MINERvA is an experiment at Fermilab dedicated to the study of neutrino–nucleus interactions in the regime of incident neutrino energies from one to few GeV. The experiment recorded neutrino and antineutrino scattering data with the NuMI beamline from 2009 to 2019 using the Low-Energy and Medium-Energy beams that peak at 3GeV and 6GeV, respectively. This article reviews the broad spectrum of interesting nuclear and particle physics that MINERvA investigations have illuminated. The newfound, detailed knowledge of neutrino interactions with nuclear targets thereby obtained is proving essential to continued progress in the neutrino physics sector.

Contents

1	Introduction	4244
2	MINERvA experiment and flux predictions	4244
3	Incoherent neutrino–nucleus interactions	4245
3.1	First measurements of quasielastic and quasielastic-like cross-sections	4245
3.2	Initial-state correlations and 2p2h-like enhancement	4247
3.3	State-of-the-art quasielastic-like measurements	4248
3.4	Charged-current pion production	4250
3.5	Kaon production	4252
3.6	Inelastic reactions	4252
4	Coherent interactions	4253
5	Conclusions and outlook	4253
	References	4255

1 Introduction

Neutrinos with energies of a few GeV are involved in many different ways among phenomena that present opportunities to probe fundamental aspects of physical reality. Neutrinos produced in accelerators play a central role in precision measurements of the oscillation parameters such as the Dirac CP-violating phase that may be present in the neutrino flavor-mixing matrix [1–4]. Measurement of a non-zero Dirac phase could unlock the mystery of the matter-antimatter asymmetry of the Universe. Neutrino beams serve as potential sources of beyond-Standard-Model (BSM) particles, such as light dark matter and heavy neutral leptons [5,6]. On the other hand, neutrinos could impede the discovery of such new forms of matter by mimicking their BSM signatures. This possibility exists because some neutrino SM processes in detector materials have aspects that are poorly known. Atmospheric neutrinos that are born in cosmic-ray-induced hadronic cascades in the upper atmosphere propagate through the Earth [7], presenting complications as well as opportunities for new physics searches. Atmospheric neutrinos oscillate, and their oscillations undergo highly interesting alterations due to propagation through a matter field. However, these highly penetrating particles also create background to rare-event searches (such as proton decay [8,9]) in deep underground experiments. Understanding how a neutrino interacts with a nucleus is essential for exploiting these opportunities. Given that current GeV-neutrino sources (accelerators or atmospheric) are not monoenergetic, these energy-sensitive interactions are convolved with the neutrino flux, causing major systematic uncertainties in precision measurements.

Neutrino–nucleus (ν -A) interactions arise not only from the primary nucleon-level interaction, but also from the effect that the nuclear environment exerts

on the initial-state nucleons and the final-state particles. Since a theory of the complete nuclear response in neutrino–nucleus interactions in the few-GeV regime of incident neutrino energy is yet to be developed [10], comprehensive ν -A measurements are needed to guide and benchmark the development of models. MINERvA (Main INjector ExpeRiment for ν -A) at Fermilab is a dedicated experiment to illuminate the interplay between hadronic and nuclear degrees of freedom in ν -A interactions and to measure aspects of intranuclear dynamics that are prerequisites for precision neutrino oscillation measurements.

MINERvA received the NuMI (Neutrinos-from-the-Main-Injector) beam at a distance of 1km from the target of the 120-GeV primary proton beam at Fermilab. In the Low-Energy (LE) beam configurations operated between 2009 and 2012, both the ν_μ and $\bar{\nu}_\mu$ fluxes peak at ~ 3 GeV, while in the Medium-Energy (ME) configurations used between 2013 and 2019, the fluxes peak at ~ 6 GeV. In both beams, there is a high-energy component that extends beyond 50GeV. The data collected by MINERvA correspond to 4.0 (1.7) and 12.1 (12.4) times 10^{20} protons on target (POT) for the LE and ME ν_μ ($\bar{\nu}_\mu$) configurations, respectively. In the Sections below, the neutrino interaction physics investigated by MINERvA is reviewed, with the main focus being the techniques developed and measurements reported that are based on the Low-Energy data set.

2 MINERvA experiment and flux predictions

The MINERvA detector [11] utilizes extruded plastic scintillator as its tracking medium. Most of the active mass is located in its central polystyrene target whose 5.4-t fiducial volume serves as a charged-particle tracker. The upstream section of the detector consists of a series of passive targets (helium, carbon, water, iron, and lead) interleaved with tracking planes. Sampling calorimeters surround both passive and active target regions. Muons produced by ν -A charged-current (CC) interactions in the tracker or in the upstream targets exit the downstream end of the tracker. These muons may then enter and propagate through the magnetized MINOS near detector [12] located 2m downstream, allowing their trajectories to be momentum-analyzed.

The downstream tracking of muons in the MINOS near detector provides an 8% muon momentum resolution (at 5GeV/ c). This complements the three-dimensional tracking and energy-loss measurement of final-state particles that is afforded by the MINERvA tracker. In the tracker, the momentum resolution for protons is 2% at 1GeV/ c with a 450-MeV/ c tracking threshold. The hadronic energy response of the detector was calibrated using test-beam measurements [13], with pion calorimetric energy resolution in the range 20–30%. Furthermore, the tracker is large compared to

^ae-mail: xianguo.lu@physics.ox.ac.uk (corresponding author)

the interaction length of the neutrons (approximately 10cm at 20MeV) produced in ν -A interactions. The 1.5-MeV detection threshold for measuring energy deposit allows interacting neutrons to be registered for a time-of-flight measurement [14]. The neutron timing resolution is 4.5ns where the hit resolution alone is 3ns from electronics effects.

The NuMI beam fluxes used by MINERvA are modeled with GEANT4 predictions that are adjusted to match hadron production data [15]. The large fiducial volume of the MINERvA tracker and the intense beam fluxes make it possible to use neutrino scattering on atomic electrons, $\bar{\nu}_\mu e^- \rightarrow \bar{\nu}_\mu e^-$, to further constrain the flux predictions. In the data from the LE (ME) NuMI beam configurations, 135 (810) neutrino–electron scattering events were identified [16,17]. The constraints thereby provided reduce the ν_μ flux normalization in the a priori prediction by 6% for LE, and 10% for ME (Fig. 1). Moreover, the uncertainty at the flux peak is reduced from 9 to 6% for LE, and from 8 to 4% for ME. In addition, the “low- ν ” method has been used to constrain the flux shape [18,19]. The latter method exploits the minimal neutrino energy dependence of the inclusive charged-current cross-section at low hadronic recoil energy.

3 Incoherent neutrino–nucleus interactions

In the few-GeV regime, neutrino–nucleus cross-sections are dominated by incoherent processes in which the constituent nucleons can be ejected, possibly accompanied by pions and other mesons. These primary processes are quasielastic (QE), baryon resonance production (RES) including non-resonant background, and deep inelastic scattering (DIS), in ascending order of excitation by incident neutrinos of increasing lab-frame energies. The initial energy and momentum of the struck nucleon and its correlation with other nucleons (including long-range correlations and two-particle-two-hole excitations, or 2p2h [20–24]) contribute to the initial-state conditions. The primary hadronic final-state particles propagate inside the remnant nucleus and may participate in final-state intranuclear interactions (FSI). The latter interactions may further excite the remaining system, causing nucleon emission or even spallation. Since pions can be absorbed or created during FSI, there is no unique experimental signature for a given primary process. As a result, the particle content and energy budget of a ν -A interaction varies with the initial and final states together with the primary reaction.

By restricting the final-state topology, MINERvA can examine exclusive and semi-inclusive reactions such as mesonless (i.e., quasielastic-like), pion, and kaon production; the experiment can study inclusive scattering as well. The exclusive-channel studies must take into account pion absorption through FSI, which enables resonance production and DIS reactions to be present in quasielastic-like topologies.

The MINERvA data enable the elucidation of one-particle-one-hole mechanisms that are generally used in ν -A scattering models, and they also allow examination of the significant 2p2h contributions to the quasielastic-like process. Concerning the latter, MINERvA has identified a 2p2h-like enhancement that simultaneously describes both neutrino and antineutrino scattering data at the kinematic region between quasielastic and resonance production. These unmodeled additional event rates are likely an admixture of all three reactions and their precise nature is still under study.

Decoupling the primary process and medium effects is challenging, especially in a wide-band neutrino beam where the neutrino energy (E_ν) is unknown. In first order, reaction E_ν -dependence comes from the primary interactions and the final-state momenta and angles depend strongly on E_ν . The nuclear response, on the other hand, affects these elementary distributions as a perturbation; it depends on E_ν through the medium coupling to the primary initial-and final-state hadrons. With a neutrino beam where the neutrino direction is precisely known, the kinematics projected onto the transverse plane to the neutrino will have less dependence on E_ν .

In a charged-current measurement, certain final-state correlations of the lepton and the hadronic system, such as the transverse kinematic imbalance (TKI) [25,26], avoid or cancel the primary-level dependence on, for example, E_ν and axial form factors, and are directly sensitive to the nuclear response with minimal dependence on the neutrino energy. Since exclusivity can be achieved in the transverse plane to the neutrino direction, TKI can probe the hidden dynamics inside the target nucleus. MINERvA has systematically explored the potential of TKI to identify the medium properties and interaction dynamics in exclusive processes.

A review of MINERvA’s measurements of incoherent interactions is presented in this section. These measurements encompass both exclusive and elastic reactions to inclusive and inelastic processes.

3.1 First measurements of quasielastic and quasielastic-like cross-sections

The charged-current quasielastic interaction (CCQE) is an important channel in neutrino oscillation experiments. This interaction gives rise to the majority of events in T2K [1] and to a sizable fraction of the events recorded by NOvA [2]. In quasielastic scattering, the neutrino energy can in principle be inferred from the outgoing lepton kinematics. However, this relatively simple interaction incurs significant effects from the nuclear environment.

Candidate CCQE interactions of neutrinos and antineutrinos on nucleons, $\nu_\mu n \rightarrow \mu^- p$ and $\bar{\nu}_\mu p \rightarrow \mu^+ n$, respectively, were extracted from the Low-Energy data in the first two cross-section measurements reported by MINERvA [27,28]. After subtracting the non-QE background processes, namely resonance pro-

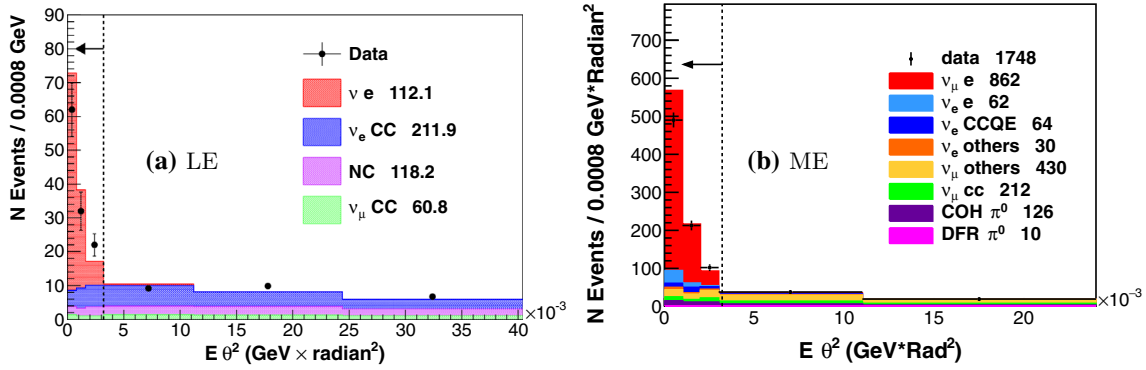


Fig. 1 Reconstructed electron energy (E) times the square of the electron angle with respect to the beam (θ) for the neutrino–electron elastic scattering candidates with the NuMI **a** LE and **b** ME configurations. Left of the dash lines are the selected samples. Stacked histograms are the simu-

lated event contributions using the a priori flux models (NC refers to other neutral-current events that are background. COH and DFR stand for coherent and diffractive production, respectively). Figures from Refs. [16, 17]

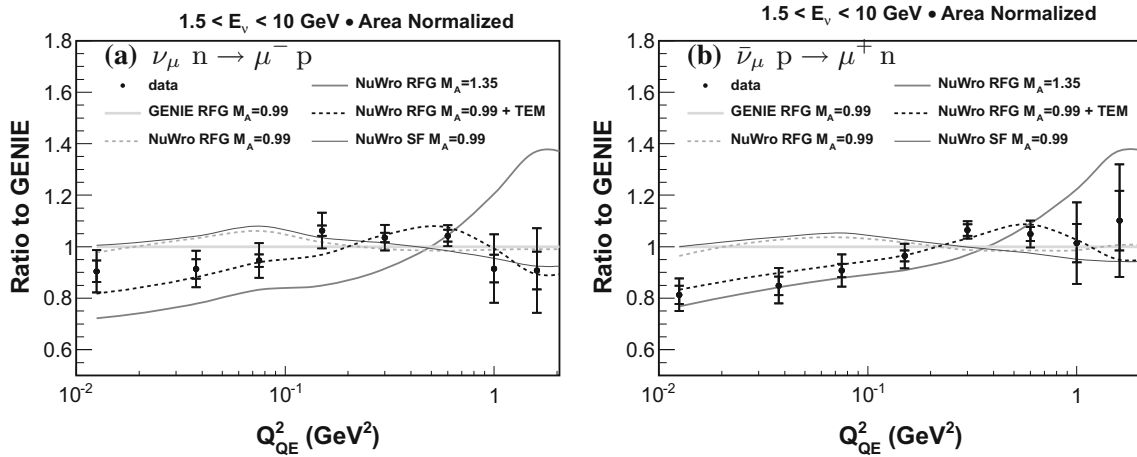


Fig. 2 **a** The ν_μ and **b** $\bar{\nu}_\mu$ CCQE cross-section in Q^2_{QE} . The subscript QE refers to the quasielastic hypothesis that uses only the muon kinematics in the calculation where the target nucleon is assumed to be at rest. The data and

model predictions are area-normalized (shape comparison only) and shown as ratios relative to GENIE. Figures from Refs. [27, 28]

duction and DIS, the flux-integrated differential cross-sections in four-momentum transfer squared, Q^2 , were compared to model predictions by GENIE [29] and NuWro [30] (Fig. 2). In the neutrino generator predictions, the shape of the Q^2 distribution is parameterized by the axial vector mass, M_A , plus model representations of the nuclear state (relativistic Fermi gas, or RFG [31], and Spectral Function, or SF [32]). Both the neutrino and antineutrino data sets were found to favor a parametric enhancement in the magnetic form factor (Transverse Enhancement Model, or TEM [33]), in addition to the *at-that-time-standard* choice of RFG and the world-average M_A value of $0.99\text{GeV}/c^2$. Since TEM is extracted from a fit to electron scattering data to describe the contributions from two-nucleon knockout processes, these results suggest possible contributions from 2p2h in neutrino and antineutrino scattering. This interpretation is further supported by the observed

pattern of energy deposits near the interaction vertices (vertex energy) in both measurements.

MINERvA also measured the ν_e CCQE cross-section in the Low-Energy neutrino data set [34]. In the Standard Model, lepton couplings are universal. However, because the final-state lepton mass is different in ν_e versus ν_μ CC events, the nuclei respond to slightly different phase spaces—a difference that cannot be ignored in oscillation experiments [35]. As the CC-induced electrons are reconstructed in the tracker which is charge-insensitive, a flux-averaged cross-section including limited contributions from $\bar{\nu}_e$ is obtained. By comparing to the ν_μ counterpart [28], it has been shown that the two CCQE cross-sections are consistent (Fig. 3). Moreover, GENIE describes the ν_e -to- ν_μ cross-section ratio within the experimental error which is of order 10–20%.

In MINERvA quasielastic measurements, the inelastic background arising from primary pion production that is followed by absorption during FSI must be

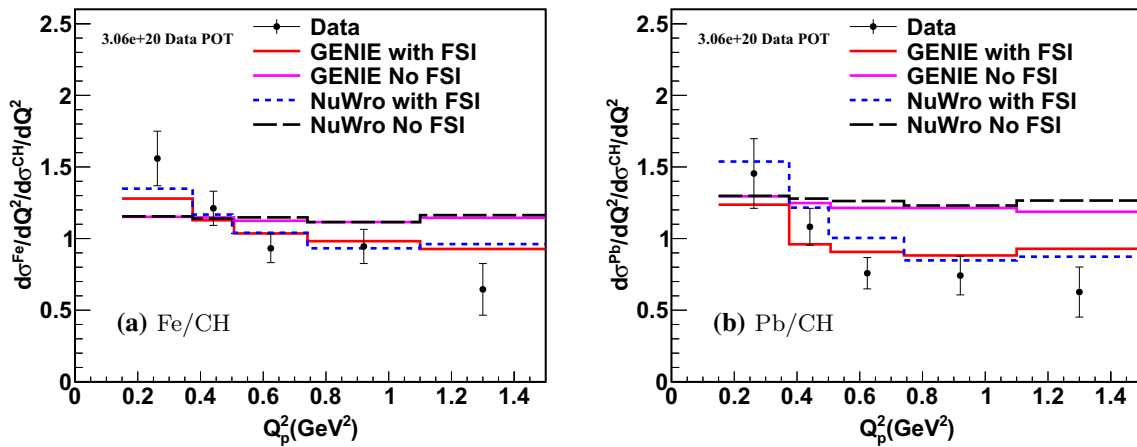


Fig. 5 The ν_μ CCQE-like per-nucleon cross-sections for **a** iron and **b** lead relative to CH as a function of Q^2 . GENIE and NuWRO predictions with RPA and 2p2h models (including the 2p2h-like enhancement discussed in Sect. 3.2) are compared. Figures from Ref. [42]

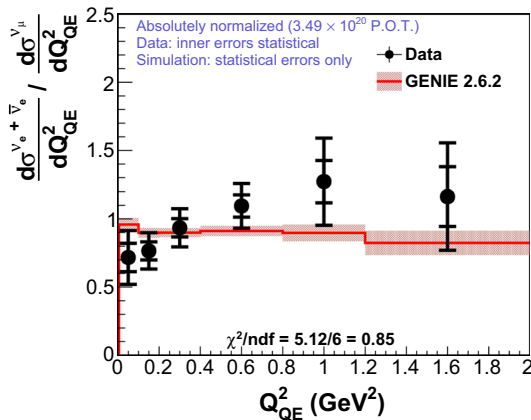


Fig. 3 Flux-integrated ν_e (dominant) and $\bar{\nu}_e$ combined CCQE cross-section divided by the ν_μ counterpart, compared to the GENIE prediction. Figure from Ref. [34]

subtracted. In subsequent MINERvA studies of the quasielastic dynamics, the inelastic pionless events are instead considered as part of the “QE-like” signal definition to mitigate the model uncertainties for pion absorption. In MINERvA’s first QE-like cross-section measurement [36], the Q^2 distribution is extracted. In addition to the change of signal definition, the Q^2 calculation is completely hadron-based, using only the momentum of the leading final-state proton above the tracking threshold. This was the first MINERvA measurement to use reconstructed proton tracks. The distribution is compared to model predictions to test different hypotheses concerning initial-state correlations and the data are found to disfavor the modeled correlations (Fig. 4).

On the other hand, proton kinematics such as the proton-based Q^2 are sensitive to FSI whose strength depends on the size of the target nucleus due to the intranuclear energy loss. This motivated further quasielastic-like cross-section measurements by MINERvA using the detector’s upstream target planes

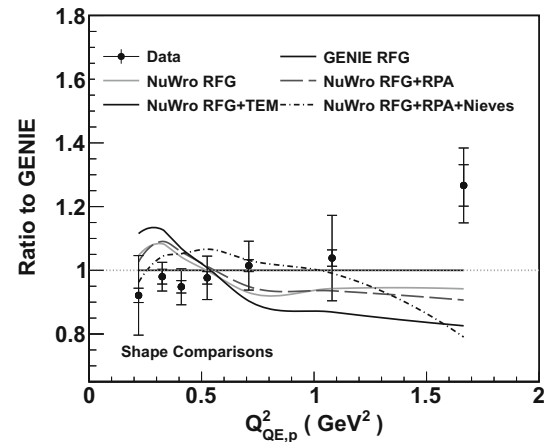


Fig. 4 The ν_μ CCQE-like cross-section in $Q^2_{QE,p}$. The additional subscript p denotes the pure hadronic calculation only using the final-state proton momentum. Comparisons are made to generator predictions that include TEM, Random Phase Approximation (RPA) [37,38], and the Valencia 2p2h model by Nieves et al. [23,39–41] (Sect. 3.2). Figure from Ref. [36]

(carbon, iron, and lead) together with the active tracker (CH) [42]. The extracted cross-section ratios of iron and lead to CH are shown in Fig. 5. The data are found to be reasonably well described by the A -dependent FSI prescriptions used by the GENIE and NUWRO event generators.

3.2 Initial-state correlations and 2p2h-like enhancement

The nuclear response are often described theoretically using the energy transfer, q_0 (also called ω or ν in the literature), and the three-momentum transfer, q_3 or $|\mathbf{q}|$, from the lepton to the target nucleus, whereby $q_3^2 - q_0^2 = Q^2$. However, the estimation of q_0 experimentally introduces uncertainties due to missing energy

from nucleon unbinding and neutrons in the final state. To avoid systematic errors that may enter in this way, MINERvA introduced a new observable called “available energy”, E_{avail} , as a proxy for q_0 in the “low-recoil” (meaning $q_3 < 0.8 \text{ GeV}$) analyses using the Low-Energy ν_μ and $\bar{\nu}_\mu$ CC inclusive samples [43, 44]. Available energy is defined as the sum of the energies from final-state particles that can be calorimetrically measured in the scintillator and excludes removal energy and neutron energy. An estimate of q_0 is still used with muon kinematics to calculate E_ν and then q_3 , but its model uncertainties are subdominant for q_3 .

The measured distributions for reconstructed E_{avail} of ν_μ scattering [43] are shown in Fig. 6(I) for two regions of the reconstructed q_3 . They are compared to the default simulation based on GENIE with modifications to pion production [45, 46]. The simulation is further improved by taking into account initial-state correlations: the collective long-range medium effect in quasielastic events calculated with a Random Phase Approximation (RPA) approach [37], and the Valencia QE-like 2p2h model [23, 39–41]. Inclusion of RPA brings the event rates at low E_{avail} into better agreement with the data, though beyond-Fermi-gas models may have a similar effect [47, 48]. The Valencia 2p2h model helps reduce the model deficit at the dip region between quasielastic and resonance production. The best data-model agreement is achieved by separately scaling up the 2p2h event rates in regions of q_0 and q_3 : across all q_0 - q_3 regions, an enhancement by 50% is required to enable the model to match the data, and in the dip region an enhancement of a factor of 2 is needed. Since this ad hoc enhancement is based on the Valencia 2p2h model, it was first interpreted as a correction to the modeled 2p2h mechanism. The GENIE model that has evolved to this end is denoted as MNvGENIE in subsequent MINERvA publications.

The corresponding $\bar{\nu}_\mu$ measurement [44] is shown in Fig. 6(II), where the aforementioned default simulations and MNvGENIE are compared in (II.a) and (II.b), respectively. Importantly, the 2p2h enhancement in MNvGENIE is only tuned to the ν_μ measurement. Consequently, its predictive power for $\bar{\nu}_\mu$, coming from the same underlying q_0 - q_3 -dependence as for ν_μ , is intriguing. It suggests that the enhancement is at the level of structure functions rather than of FSI or Fermi motion. However, given its empirical nature, this enhancement should be understood as 2p2h-like; the analysis does not currently rule out a quasielastic or resonant enhancement in addition to 2p2h.

The inclusion of RPA and 2p2h in the predictions has made a significant improvement in the description of the MINERvA data. The evolution of modeling improvement from GENIE to MNvGENIE is illustrated by a reanalysis of the vertex energy in a ν_μ CCQE-like sample [49]. As is shown in Fig. 7, the distributions of the reconstructed vertex energies in events with and without proton tracks are described by GENIE after the modifications with RPA, Valencia 2p2h, and the 2p2h-like enhancement are taken into account.

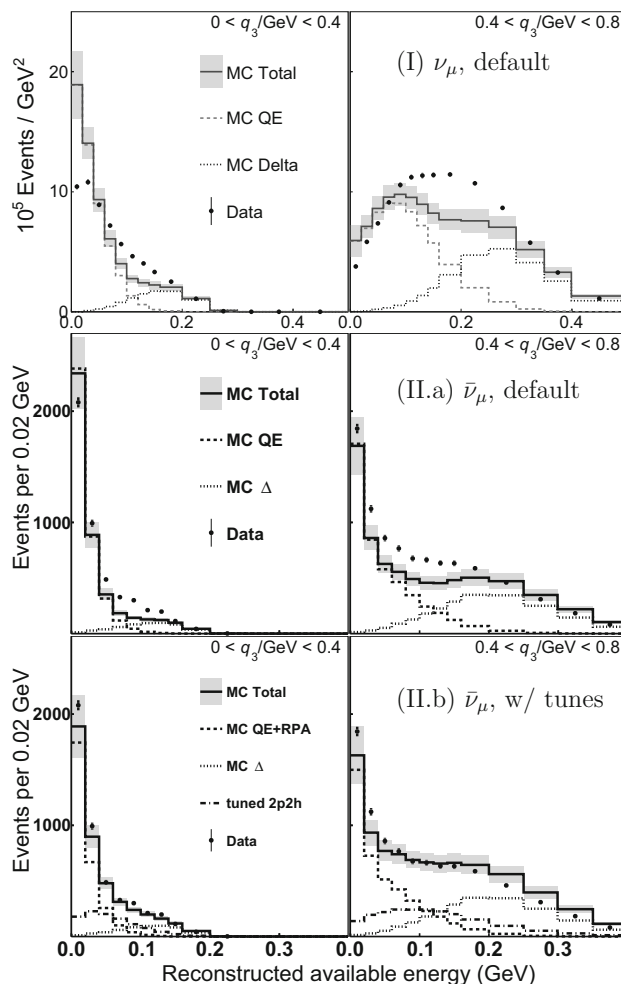


Fig. 6 Event distributions in the reconstructed E_{avail} for two ranges of the reconstructed q_3 in (I) ν_μ and (II) $\bar{\nu}_\mu$ charged-current inclusive samples. In (I) and (II.a) the default simulations (see text) are used, while in (II.b) the predictions with the ν_μ -based tunes (MNvGENIE) are shown. In the legend, the resonance region is labeled as Delta (Δ). Figures from Refs. [43, 44]

3.3 State-of-the-art quasielastic-like measurements

In the few-GeV range of the neutrino energy, the quasielastic cross-section is nearly constant as a function of E_ν , while the phase space for resonance production and DIS is opening up. In addition to extracting the CCQE-like cross-sections in Q^2 and E_ν which can be calculated with the quasielastic hypothesis (that is invalid for the non-QE components), MINERvA measured the CC muon transverse (p_T) and longitudinal momenta ($p_{||}$) using the Low-Energy $\bar{\nu}_\mu$ [50], ν_μ [49], and Medium-Energy ν_μ [51] data sets. These particular muon momentum projections respectively approximate the true Q^2 and E_ν . As shown in Fig. 8 for the Low-Energy ν_μ results, the different interaction contributions in the MNvGENIE predictions are relatively stable across the $p_{||}$ bins. This is in contrast to the inclusive measurement discussed in Sect. 3.6 below where the $p_{||}$ -

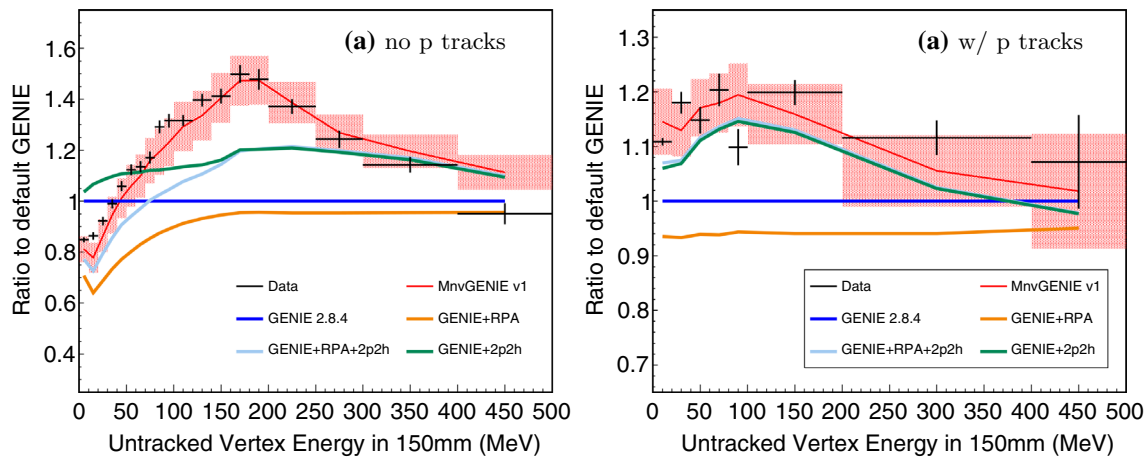
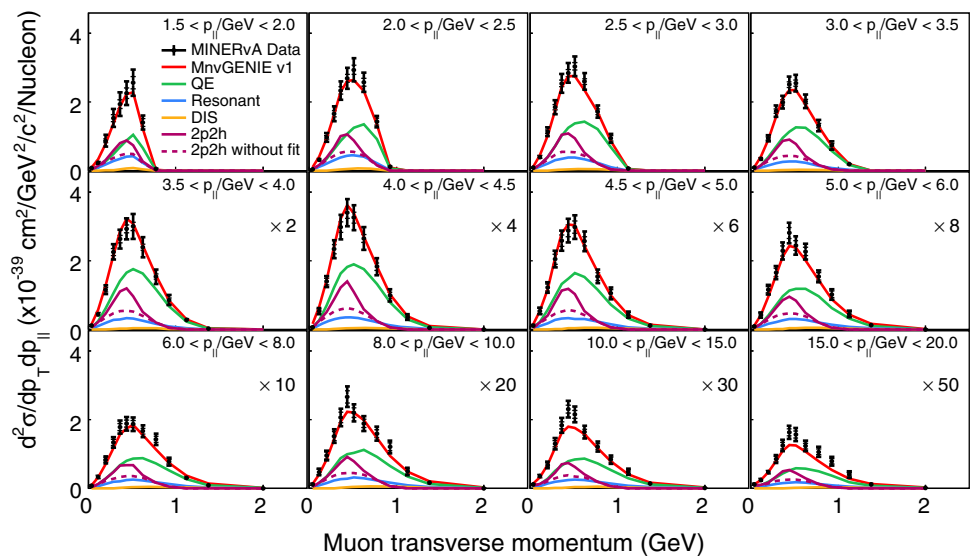


Fig. 7 Ratio of the data and various GENIE predictions to GENIE 2.8.4 as a function of the reconstructed vertex energy in ν_μ CCQE-like events **a** without and **b** with pro-

ton tracks. The 2p2h-like enhancement can be seen by comparing MnvGENIE and “GENIE +RPA+(Valencia)2p2h”. Figures from Ref. [49]

Fig. 8 ν_μ CCQE-like cross-sections in p_T in bins of $p_{||}$. Unstacked curves show the various components of the MnvGENIE predictions. “2p2h without fit” refers to the Valencia model while “2p2h” includes the ad hoc enhancement discussed in Sect. 3.2. Figure from Ref. [49]



(and therefore, E_{ν^-}) dependence of the DIS processes is evident. In both the QE-like and the inclusive measurements, while MnvGENIE describes the data in most bins, there is an overall model deficit at large $p_{||}$.

By measuring the transverse kinematic imbalance which cancel out the primary interaction kinematics, the cross-section dependence on the incoming neutrino energy is lessened and also the initial-and final-state effects can be directly probed [26]. Using the ν_μ CCQE-like events in the tracker with the Low-Energy data [52], the direction and magnitude of the transverse momentum imbalance ($\delta \mathbf{p}_T$) between the muon and the leading proton, $\delta \alpha_T$ and δp_T , respectively, are calculated. The angle $\delta \alpha_T$ has the most sensitivity to FSI and to the unaccounted-for momentum carried by missing particles such as absorbed pions or the correlated nucleon of the proton from 2p2h. Figure 9 shows that, within the uncertainties, MnvGENIE describes the data. Here, FSI are classified into three categories:

1. A flat distribution for events which do not experience FSI (both the “no-FSI” and “p-FSI non-interacting” categories in Fig. 9) reflecting the isotropy of the Fermi motion;
2. The deceleration region ($\delta \alpha_T \rightarrow 180^\circ$) for energy-dissipating processes—decelerating FSI, pion absorption, and 2p2h;
3. The acceleration region ($\delta \alpha_T \rightarrow 0^\circ$) for accelerating FSI if such a mechanism exists.

Interestingly, GENIE did predict FSI acceleration for protons, roughly half of them singularly occupying the acceleration region, while the other half falls into the deceleration region due to the transverse projection.

By assuming a carbon-11 target remnant, the transverse momentum imbalance magnitude δp_T is promoted to the three-dimensional momentum imbalance, p_n , following from an additional constraint by energy conservation [53]. For the FSI-noninteracting events, p_n can

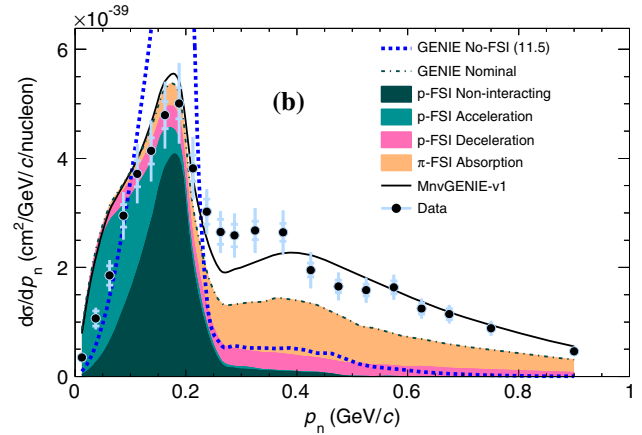
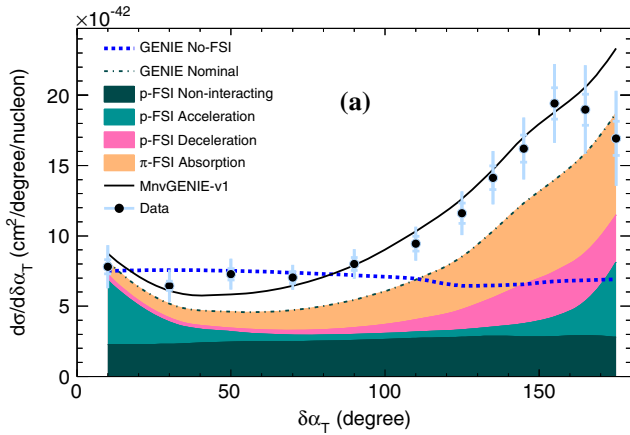


Fig. 9 Differential cross-sections for ν_μ CCQE-like events in **a** $\delta\alpha_T$ and **b** p_n . The stacked colored histograms depict categories of FSI and sum up to the GENIE nominal predictions. The predicted 2p2h component including the

2p2h-like enhancement can be inferred from the difference between MnvGENIE and the nominal GENIE. Figures from Ref. [52]

be interpreted as the momentum of the struck neutron in the CCQE initial state. The location of the Fermi-motion peak in data is well captured by the MnvGENIE prediction. However, its accelerating FSI component causes the predicted peak shape to deviate from data. This component was identified as the elastic component of the GENIE v2.8 hA FSI model and has been removed in later versions of GENIE [54, 55]. The measured cross-section is further compared to NuWRO predictions with alternative nuclear states: local Fermi gas (LFG) and Spectral Function. The latter model better describes the Fermi motion peak, but neither model provides enough strength in the transition region between the quasielastic peak and the non-QE tail [52].

An enhanced sensitivity to another initial-state condition, the binding energy, is achieved by further projecting $\delta\mathbf{p}_T$ onto the lepton scattering plane, which defines the δp_{TY} variable [55]. Various generator implementations of the interaction energy on carbon are compared (Fig. 10) and the data favor approximate corrections to GENIE [56].

3.4 Charged-current pion production

Neutrino-induced pion production is an important channel in neutrino oscillation experiments because it accounts for a large part of the signal in NOvA and DUNE [3] far detector event samples, and is both a low-statistics signal and background in the far detector samples of T2K. The process can proceed through baryon resonance production or through non-resonant interaction. It can also occur through a CC coherent interaction with a nucleus—see discussions in Sect. 4. Because of the additional final-state hadrons, incoherent pion production may be more affected by the nuclear environment than the quasielastic process, and the difficulty with reconstructing pions means that the process is harder to measure. One would like to use the lessons learned about nuclear effects in quasielastic-like scatter-

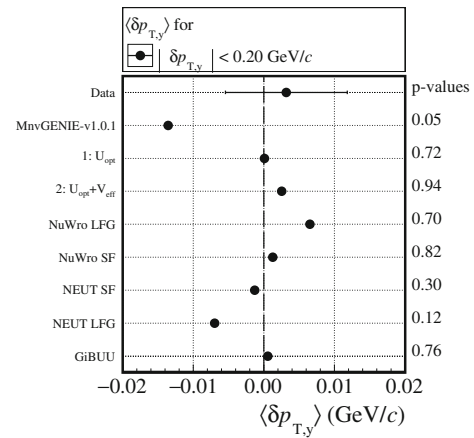


Fig. 10 Mean δp_{TY} calculated from the ν_μ CCQE-like differential cross-section in δp_{TY} within -0.20 to 0.20 GeV/c . The p -value is the probability, assuming normal distribution, that the observed result would have been produced by the test model. U_{opt} and V_{eff} are the optical and Coulomb potentials experienced by the CCQE proton and muon, respectively, as proposed in Ref. [56]. NEUT [57] and GiBUU [58] predictions are also compared. Figure from Ref. [55]

ing to (overt) pion production, but the effects may not be the same. The nuclear responses to the pion production fall into three categories according to their relation with those of the quasielastic-like processes:

1. Nuclear responses that are generic but might be quantitatively different in pion production are Fermi motion, binding energy, initial-state correlations, and Pauli blocking [59, 60];
2. Pion absorption and charge exchange are nuclear responses that migrate primary pion production channels among each other and into quasielastic-like topology [61, 62];

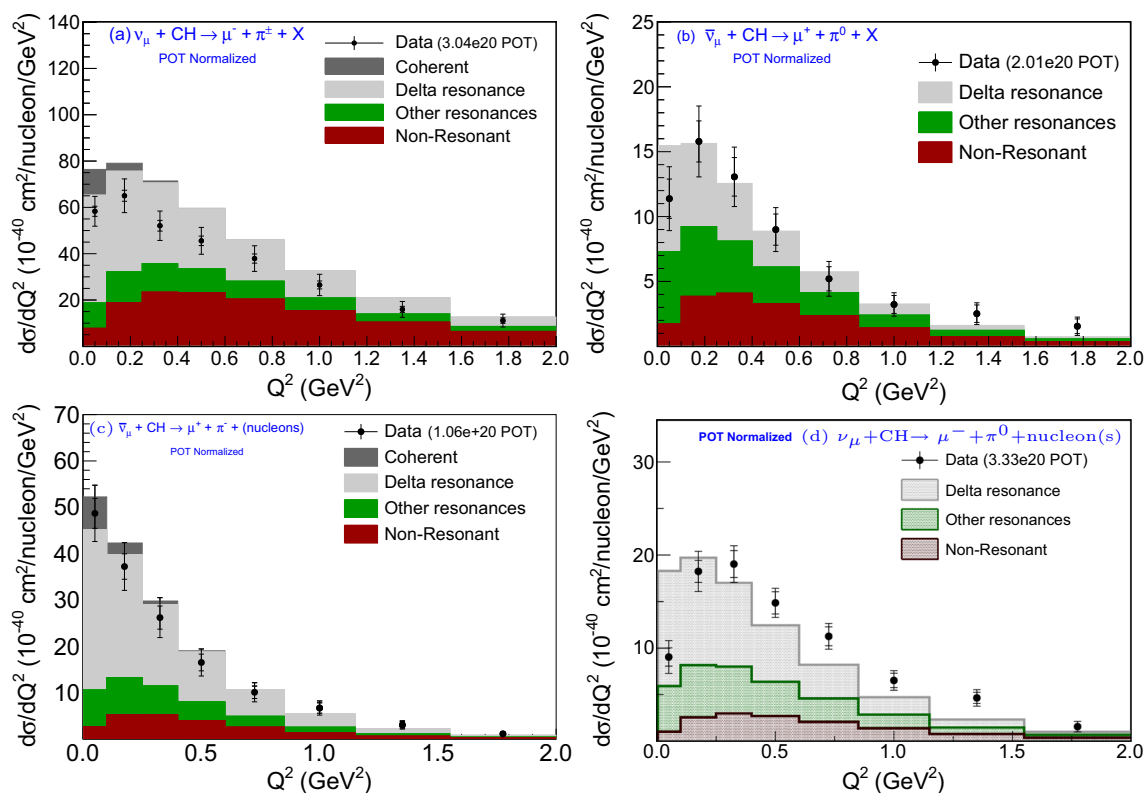


Fig. 11 Cross-sections in Q^2 for **a** $\nu_\mu \pi^+$ (with limited contributions from π^-), **b** $\bar{\nu}_\mu \pi^0$, **c** $\bar{\nu}_\mu \pi^-$, and **d** $\nu_\mu \pi^0$ charged-current productions compared to GENIE predictions. Figures from Refs. [67,68,71]

3. Some nuclear responses are specific to pion production such as Δ -resonance in-medium modifications [63–65].

Moreover, in the energy region of MINERvA, the contribution of higher resonances could be important along with the nuclear medium effects in the pion production processes. MINERvA has measured the following processes on its plastic scintillator tracker with the Low-Energy beam:

- ν_μ CC π^+ production (with limited contributions from π^-) [66,67],
- ν_μ CC single π^0 production [68,69],
- $\bar{\nu}_\mu$ CC single π^0 production [67,70], and
- $\bar{\nu}_\mu$ CC single π^- production [71].

The nuclear effects described by RPA and 2p2h are crucial to the description of quasielastic-like processes in MINERvA (Sect. 3.2). Since the RPA effect creates a suppression of the QE-like cross-section at low Q^2 , measuring Q^2 in pion production could provide relevant information. However, as shown by the results in Fig. 11, suppression at low Q^2 ranges from being nonexistent ($\bar{\nu}_\mu \pi^-$ [71]), to mild or insignificant ($\nu_\mu \pi^+$ [66,67] and $\bar{\nu}_\mu \pi^0$ [67,70]), and to fairly pronounced ($\nu_\mu \pi^0$ [68]). A combined fit of the various underlying mechanisms using a subset of these measurements can

be found in Ref. [72]. On the other hand, while 2p2h in pion production has not been incorporated into predictions, current models describe the MINERvA data with sufficient strength without it. The effect of initial-state correlations on pion production is not well understood.

Because of the granularity of the tracker and the event statistics obtained for ν_μ charged-current proton- π^0 final states with the Low-Energy beam, MINERvA is able to investigate the transverse kinematic imbalances that may arise in pion production [69]. In this way, MINERvA can probe the initial state and FSI in parallel to the CCQE-like measurement discussed in Sect. 3.3 (Fig. 12). The TKI between the muon and the $p\text{-}\pi^0$ hadronic system is calculated by reconstructing the π^0 momentum and combining it with the proton momentum [73]. As with ν_μ CCQE, this channel also has an initial-state neutron and as expected, the Fermi motion peaks in Fig. 12b from both channels are consistent. The consistency in the p_n tail size and in the trend of $\delta\alpha_T$ in Fig. 12 is purely coincidental. As a specific example, if nature had less pion absorption, the QE-like p_n tail and the $\delta\alpha_T$ deceleration region would fall but the overall π^0 production would increase. Currently, for the same Fermi motion peak, generator model predictions do not describe both channels simultaneously [69], clearly illustrating the challenges inherent to consistent modeling of few-GeV ν -A interactions.

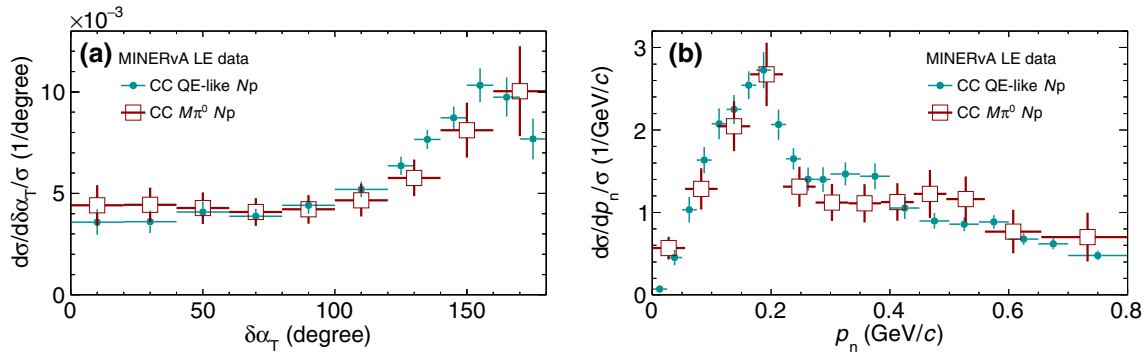
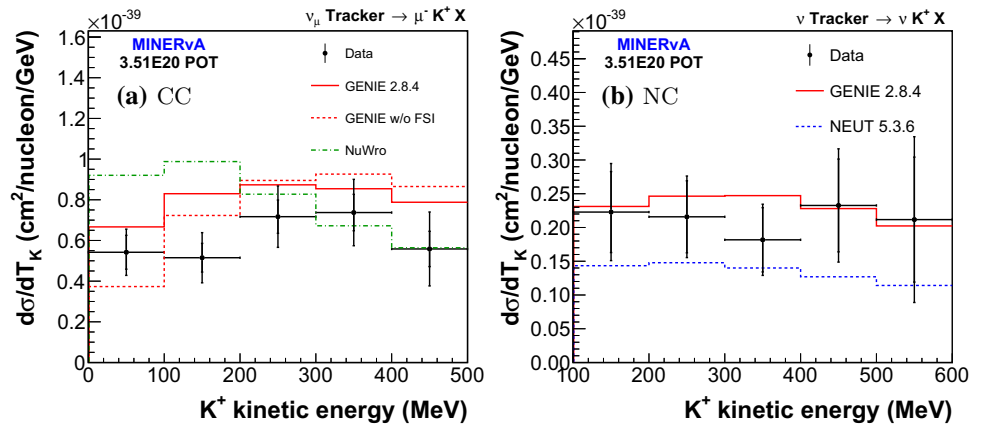


Fig. 12 Differential cross-sections in **a** $\delta\alpha_T$ and **b** p_n for ν_μ charged-current $p\text{-}\pi^0$ production, compared to quasielastic-like scattering [52,55] (Sect. 3.3). The data sets are area-normalized. Figures from Ref. [69]

Fig. 13 Charged-current **a** and neutral-current **b** ν_μ K^+ production cross-sections in kinetic energy, compared to GENIE, NuWRO, and NEUT predictions. Figures from Refs. [75,76]



3.5 Kaon production

Charged and neutral kaons are produced in both charged-current and neutral-current interactions at the beam energies of the MINERvA exposures. Kaon production is important to measure because the neutral-current (NC) channels yielding K^+ mesons constitute a background to proton decay searches [8,9]. This background arises from interactions of atmospheric neutrinos that are incident on proton decay detectors. The production mechanism is associated production with another strange meson or with a hyperon. Below the threshold of associated particle production, kaon production would take place through $\Delta S = 1$ currents (S is the strangeness quantum number). At the energies of present interest, single kaon production may be important [74]. A final-state K^+ with energy less than $\sim 600\text{MeV}$ can stop inside the MINERvA tracker and then decay at rest. Once a K^+ decay chain is identified through the decay-associated time delay, the event topology, and the energy loss, the K^+ initial momentum can be calculated from track range. For neutral-current interactions, the final-state lepton does not identify the vertex location, consequently the 100-MeV tracking threshold sets a lower limit on the measured kaon kinetic energy. For CC interactions on the other hand, the final-state muon determines the primary vertex as the K^+ starting point, hence the kaon kinetic energy threshold can be lower since a kaon track needs not

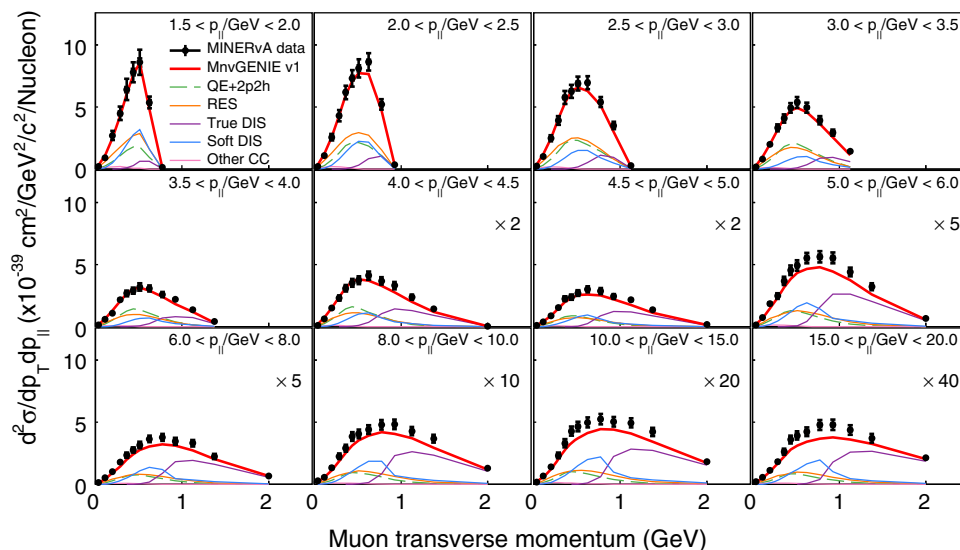
be identified. Figure 13 shows the measured charged-current [75] and neutral-current [76] cross-sections. The analysis showed that the GENIE prediction was in agreement with the neutral-current measurement, while the NEUT prediction, which was used by Super-K [8], predicted a lower cross-section by about 20%.

3.6 Inelastic reactions

In quasielastic and resonance production, the dynamic degrees of freedom are baryons and mesons. The invariant mass of the hadronic system, W , is of the order of $1\text{--}2\text{GeV}/c^2$. In the high- W high- Q^2 region where DIS dominates, the target nucleon breaks up in the reaction and the QCD dynamics in the nuclear environment can be studied. This kinematic region is only accessible in inclusive measurements where any hadronic final state is allowed.

MINERvA measures CC inclusive cross-sections using the muon kinematics. These measurements require one momentum-analyzed muon per event; no requirement is placed on the final-state hadronic system [77]. Figure 14 shows the $p_{||}$ -evolution of the inclusive p_T spectra. In contrast to the CCQE-like measurement of Fig. 8 of Sect. 3.3, there are significant contributions from (GENIE) DIS in all $p_{||}$ bins and its relative contribution increases with $p_{||}$. As in the CCQE-like case, there is an overall deficit of MNVGENIE at large $p_{||}$.

Fig. 14 ν_μ charged-current inclusive cross-sections in p_T in bins of $p_{||}$ compared to MNVGENIE predictions with unstacked contributions shown. See Fig. 8 for comparison. “True DIS” events are defined as GENIE DIS events that satisfy $W > 2 \text{ GeV}/c^2$ and $Q^2 > 1 \text{ GeV}^2$. “Soft DIS” is defined to contain the remaining GENIE DIS events. Figure from Ref. [77]



Charged-current inclusive cross-sections have also been measured in the passive target region as a function of the reconstructed Bjorken- x . These measurements are carried out for iron and lead targets; they are based on both muon kinematics and calorimetric hadronic energy [78]. The ratios of ν_μ -Fe and ν_μ -Pb cross-section to the cross-section in the tracker (CH) are shown in Fig. 15. The default GENIE simulations show a strong deficit in the elastic region (Bjorken- $x \sim 1$) which might be due to the unmodeled 2p2h contributions.

By restricting the sample to the DIS region, $W > 2 \text{ GeV}/c^2$ and $Q^2 > 1 \text{ GeV}^2$, these Bjorken- x -dependent cross-section ratios can be compared to additional DIS models [79] (Fig. 16). As is shown in Fig. 16b for Pb, the data at Bjorken- $x < 0.1$ suggests possible shadowing effects beyond those predicted. Since these models are only tuned to charged-lepton scattering data, which are by definition insensitive to the axial-vector current, these data also reflect neutrino-specific effects in the DIS region.

4 Coherent interactions

Coherent pion production is a relatively rare process that is worthy of measurement because the neutral-current channel contributes a small but poorly constrained background to electron neutrino appearance measurements. Charged-current coherent pion production, $\bar{\nu}_\mu + A \rightarrow \mu^+ + \pi^\pm + A$, can be considered as the inverse process of the pion decay permitted in a nuclear environment, in analogy to pair production in QED. The momentum transfer from the pion to the nucleus—denoted by $t \equiv (P' - P)^2$ where P' and P are the final and initial 4-momenta of the nucleus—is small and leaves the nucleus intact, and the process has a characteristic exponential fall-off of the cross-section with increasing $|t|$. By reconstructing t , MINERvA measured this process with both ν_μ and $\bar{\nu}_\mu$ beams [82].

This measurement has provided a critical validation of the model implementation in generators (Fig. 17). Further model comparisons in a reanalysis [83] show preference for the Berger–Sehgal model [84] over the Rein–Sehgal model [85,86] used by GENIE. In the low energy region, explicit nuclear model has been used to study coherent pion production (see, for example, Refs. [87,88]).

The t -measurement was augmented with K^+ tagging (Sect. 3.5) to search for the analogous kaon production, $\nu_\mu + A \rightarrow \mu^- + K^+ + A$. MINERvA found 6 candidates with 1.77 predicted background events. This observation comprises evidence at 3.0σ that CC coherent K^+ production does indeed occur [89].

A process that is the analog of neutrino NC coherent π^0 production on nuclei, is neutrino diffractive π^0 production on hydrogen: $\bar{\nu} + H \rightarrow \bar{\nu} + \pi^0 + H$. This reaction relies solely on vacuum-quantum-number (Pomeron) exchange, hence diffractive [90]. In the past, diffractive π^0 production on hydrogen was not included in neutrino event generators. It has been identified by MINERvA as the cause of a data excess observed in neutral-current events containing electromagnetic showers in the tracker [91].

5 Conclusions and outlook

With the NuMI Low-Energy data, MINERvA has investigated a wide variety of neutrino interactions in the GeV region of incident neutrino and antineutrino energies, including elastic scattering on electrons as well as neutrino–nucleus incoherent and coherent scattering processes. The reported measurements include utilization of neutrino scattering observations to constrain the flux, precision measurements of model parameters and model validation, and discoveries of novel processes. The results show neutrino–nucleus interactions to involve complex phenomena which challenge many of the current theoretical descriptions. Incre-

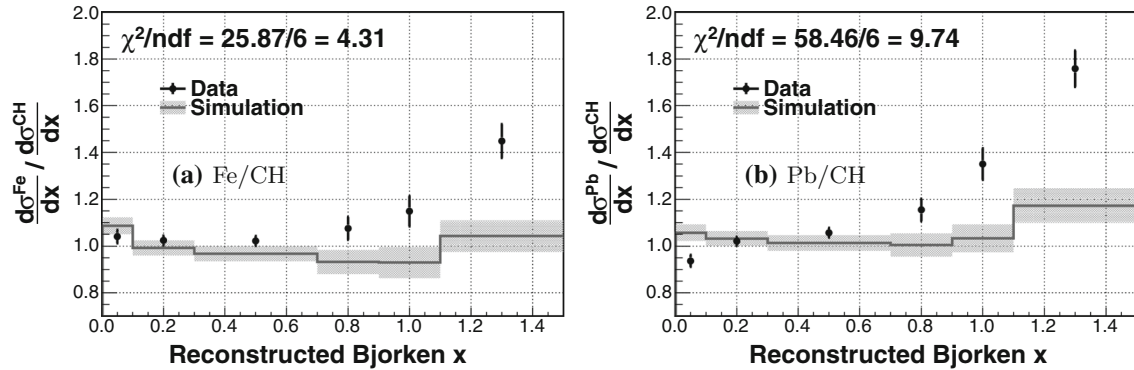


Fig. 15 Ratios of ν_μ charged-current inclusive cross-sections per nucleon as a function of the reconstructed Bjorken- x for **a** Fe/CH and **b** Pb/CH, compared to the default GENIE simulations. Figures from Ref. [78]

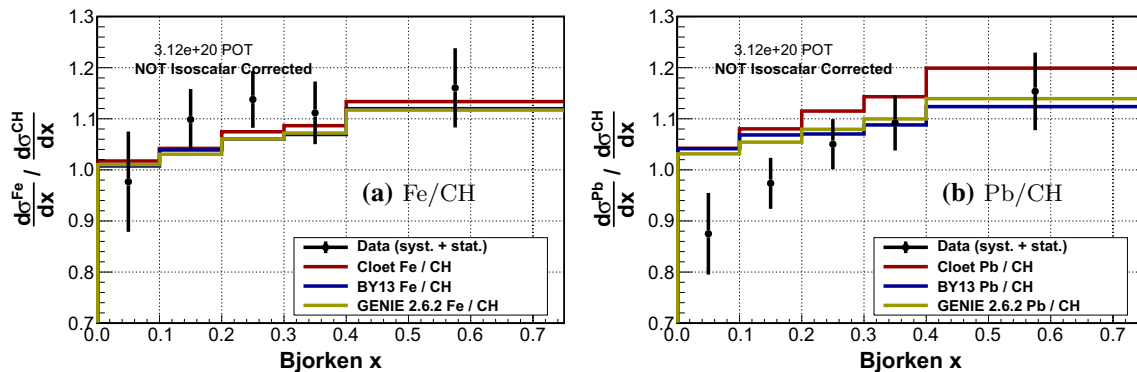
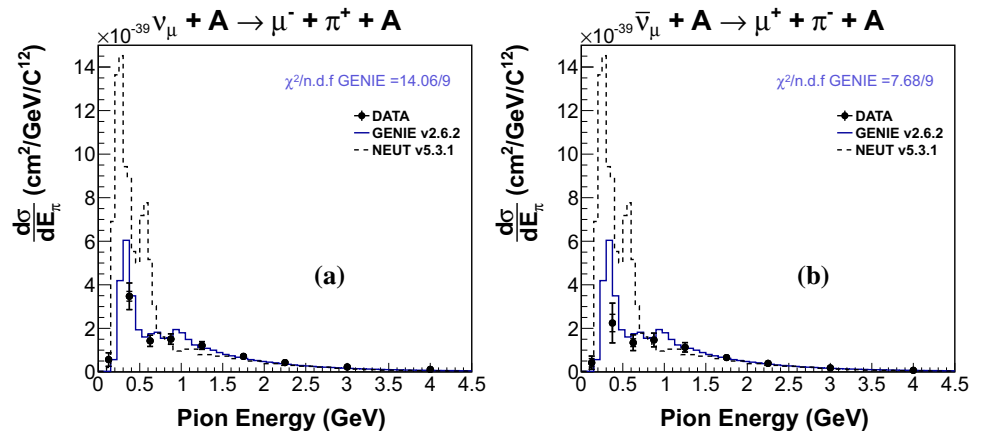


Fig. 16 Ratios of ν_μ charged-current DIS cross-sections per nucleon as a function of Bjorken- x for **a** Fe/CH and **b** Pb/CH, compared to the default GENIE, Bodek-Yang (BY13) [80], and Cloet [81] models. Figures from Ref. [79]

Fig. 17 Charged-current coherent pion production cross-sections as a function of the pion energy in **a** ν_μ and **b** $\bar{\nu}_\mu$ scattering, compared to the Rein-Sehgal model predictions implemented in GENIE and NEUT. Figures from Ref. [82]



mental improvements to the models have been essential to progress with MINERvA data and interpretation. The experiment's Medium-Energy data, analyses of which are currently underway, will enable comparisons of interaction channels on a range of nuclei at new levels of statistical precision, and expansion to kinematic phase space that has heretofore not been accessible. These data, consolidated by a preservation campaign [92,93], will not only facilitate future precision measurements of neutrino oscillations, but also further

extend the knowledge of electroweak phenomena that lie at the intersection of nuclear and particle physics.

Acknowledgements This document was prepared by members of the MINERvA Collaboration using the resources of the Fermi National Accelerator Laboratory (Fermilab), a U.S. Department of Energy, Office of Science, HEP User Facility. Fermilab is managed by Fermi Research Alliance, LLC (FRA), acting under Contract No. DE-AC02-07CH11359. These resources included support for the MIN-

ERvA construction project, and support for construction also was granted by the United States National Science Foundation under Award No. PHY-0619727 and by the University of Rochester. Support for participating scientists was provided by NSF and DOE (USA); by CAPES and CNPq (Brazil); by CoNaCyT (Mexico); by Proyecto Basal FB 0821, CONICYT PIA ACT1413, and Fondecyt 3170845 and 11130133 (Chile); by CONCYTEC (Consejo Nacional de Ciencia, Tecnología e Innovación Tecnológica), DGI-PUCP (Dirección de Gestión de la Investigación - Pontificia Universidad Católica del Perú), and VRI-UNI (Vice-Rectorate for Research of National University of Engineering) (Peru); NCN Opus Grant No. 2016/21/B/ST2/01092 (Poland); by Science and Technology Facilities Council (UK); by EU Horizon 2020 Marie Skłodowska-Curie Action; by a Cottrell Postdoctoral Fellowship from the Research Corporation for Scientific Advancement; by an Imperial College London President's PhD Scholarship. We thank the MINOS Collaboration for use of its near detector data. Finally, we thank the staff of Fermilab for support of the beam line, the detector, and computing infrastructure.

Open Access This article is licensed under a Creative Commons Attribution 4.0 International License, which permits use, sharing, adaptation, distribution and reproduction in any medium or format, as long as you give appropriate credit to the original author(s) and the source, provide a link to the Creative Commons licence, and indicate if changes were made. The images or other third party material in this article are included in the article's Creative Commons licence, unless indicated otherwise in a credit line to the material. If material is not included in the article's Creative Commons licence and your intended use is not permitted by statutory regulation or exceeds the permitted use, you will need to obtain permission directly from the copyright holder. To view a copy of this licence, visit <http://creativecommons.org/licenses/by/4.0/>.

References

1. K. Abe et al., Constraint on the matter–antimatter symmetry-violating phase in neutrino oscillations. *Nature* **580**(7803), 339–344 (2020)
2. M.A. Acero et al., First measurement of neutrino oscillation parameters using neutrinos and antineutrinos by NOvA. *Phys. Rev. Lett.* **123**(15), 151803 (2019)
3. B. Abi et al., Deep underground neutrino experiment (DUNE), far detector technical design report, volume I introduction to DUNE. *JINST* **15**(08), T08008 (2020)
4. K. Abe et al., “Hyper-Kamiokande Design Report,” (2018)
5. K. Abe et al., Search for heavy neutrinos with the T2K near detector ND280. *Phys. Rev. D* **100**(5), 052006 (2019)
6. B. Abi et al., Prospects for beyond the Standard Model physics searches at the deep underground neutrino experiment. *Eur. Phys. J. C* **81**(4), 322 (2021)
7. K. Abe et al., Atmospheric neutrino oscillation analysis with external constraints in Super-Kamiokande I-IV. *Phys. Rev. D* **97**(7), 072001 (2018)
8. K. Abe et al., Search for proton decay via $p \rightarrow \nu K^+$ using 260 kiloton-year data of Super-Kamiokande. *Phys. Rev. D* **90**(7), 072005 (2014)
9. F. An et al., Neutrino physics with JUNO. *J. Phys.* **G43**(3), 030401 (2016)
10. L. Alvarez-Ruso et al., NuSTEC 1 1 Neutrino Scattering Theory Experiment Collaboration <http://nustec.fnal.gov>. White Paper: Status and challenges of neutrino-nucleus scattering. *Prog. Part. Nucl. Phys* **100**, 1–68 (2018)
11. L. Aliaga et al., Design, calibration, and performance of the MINERvA detector. *Nucl. Instrum. Methods* **A743**, 130–159 (2014)
12. D.G. Michael et al., The magnetized steel and scintillator calorimeters of the MINOS experiment. *Nucl. Instrum. Methods A* **596**, 190–228 (2008)
13. L. Aliaga et al., MINERvA neutrino detector response measured with test beam data. *Nucl. Instrum. Methods* **A789**, 28–42 (2015)
14. M. Elkins et al., Neutron measurements from antineutrino hydrocarbon reactions. *Phys. Rev. D* **100**(5), 052002 (2019)
15. L. Aliaga et al. Neutrino flux predictions for the NuMI beam. *Phys. Rev. D* **94**(9), 092005 (2016) (**Addendum: Phys. Rev. D** **95**, no.3, 039903 (2017))
16. J. Park et al., Measurement of neutrino flux from neutrino-electron elastic scattering. *Phys. Rev. D* **93**(11), 112007 (2016)
17. E. Valencia et al., Constraint of the MINERvA medium energy neutrino flux using neutrino-electron elastic scattering. *Phys. Rev. D* **100**(9), 092001 (2019)
18. J. Devan et al., Measurements of the inclusive neutrino and antineutrino charged current cross sections in MINERvA using the low- ν flux method. *Phys. Rev. D* **94**(11), 112007 (2016)
19. L. Ren et al., Measurement of the antineutrino to neutrino charged-current interaction cross section ratio in MINERvA. *Phys. Rev. D* **95**(7), 072009 (2017) (**Addendum: Phys. Rev. D** **97**(1), 019902 (2018))
20. J. Marteau, Effects of the nuclear correlations on the neutrino oxygen interactions. *Eur. Phys. J. A* **5**, 183–190 (1999)
21. M. Martini, M. Ericson, G. Chanfray, J. Marteau, Neutrino and antineutrino quasielastic interactions with nuclei. *Phys. Rev. C* **81**, 045502 (2010)
22. J. Nieves, I.R. Simo, M.J.V. Vacas, Inclusive charged-current neutrino–nucleus reactions. *Phys. Rev. C* **83**, 045501 (2011)
23. R. Gran, J. Nieves, F. Sanchez, M.J.V. Vacas, Neutrino-nucleus quasi-elastic and 2p2h interactions up to 10 GeV. *Phys. Rev. D* **88**(11), 113007 (2013)
24. O. Benhar, A. Lovato, N. Rocco, Contribution of two-particle–two-hole final states to the nuclear response. *Phys. Rev. C* **92**(2), 024602 (2015)
25. X.-G. Lu, D. Coploue, R. Shah, G. Barr, D. Wark, A. Weber, Reconstruction of energy spectra of neutrino beams independent of nuclear effects. *Phys. Rev. D* **92**(5), 051302 (2015)
26. X.-G. Lu, L. Pickering, S. Dolan, G. Barr, D. Coploue, Y. Uchida, D. Wark, M.O. Wascko, A. Weber, T. Yuan, Measurement of nuclear effects in neutrino interactions with minimal dependence on neutrino energy. *Phys. Rev. C* **94**(1), 015503 (2016)

27. L. Fields et al., Measurement of muon antineutrino quasielastic scattering on a hydrocarbon target at $E_\nu \sim 3.5$ GeV. *Phys. Rev. Lett.* **111**(2), 022501 (2013)
28. G.A. Fiorentini et al., Measurement of muon neutrino quasielastic scattering on a hydrocarbon target at $E_\nu \sim 3.5$ GeV. *Phys. Rev. Lett.* **111**, 022502 (2013)
29. C. Andreopoulos et al., The GENIE neutrino Monte Carlo generator. *Nucl. Instrum. Methods* **A614**, 87–104 (2010)
30. T. Golan, C. Juszczak, J.T. Sobczyk, Final state interactions effects in neutrino–nucleus interactions. *Phys. Rev. C* **86**, 015505 (2012)
31. A. Bodek, J.L. Ritchie, Fermi motion effects in deep inelastic lepton scattering from nuclear targets. *Phys. Rev. D* **23**, 1070 (1981)
32. O. Benhar, A. Fabrocini, S. Fantoni, I. Sick, Spectral function of finite nuclei and scattering of GeV electrons. *Nucl. Phys. A* **579**, 493–517 (1994)
33. A. Bodek, H.S. Budd, M.E. Christy, Neutrino quasielastic scattering on nuclear targets: parametrizing transverse enhancement (meson exchange currents). *Eur. Phys. J. C* **71**, 1726 (2011)
34. J. Wolcott et al., Measurement of electron neutrino quasielastic and quasielasticlike scattering on hydrocarbon at $\langle E_\nu \rangle = 3.6$ GeV. *Phys. Rev. Lett.* **116**(8), 081802 (2016)
35. M. Day, K.S. McFarland, Differences in quasi-elastic cross-sections of muon and electron neutrinos. *Phys. Rev. D* **86**, 053003 (2012)
36. T. Walton et al., Measurement of muon plus proton final states in ν_μ interactions on hydrocarbon at $\langle E_\nu \rangle = 4.2$ GeV. *Phys. Rev. D* **91**(7), 071301 (2015)
37. J. Nieves, J.E. Amaro, M. Valverde, Inclusive quasielastic neutrino reactions. *Phys. Rev. C* **70**, 055503 (2004) (**Erratum: Phys. Rev. C** **72**, 019902 (2005))
38. K.M. Graczyk, J.T. Sobczyk, The Algebraic solution of RPA equations for the charged current quasielastic neutrino nucleus scattering. *Eur. Phys. J. C* **31**, 177–185 (2003)
39. J. Nieves, I.R. Simo, M.J.V. Vacas, The nucleon axial mass and the MiniBooNE Quasielastic neutrino–nucleus scattering problem. *Phys. Lett. B* **707**, 72–75 (2012)
40. J.T. Sobczyk, Multinucleon ejection model for meson exchange current neutrino interactions. *Phys. Rev. C* **86**, 015504 (2012)
41. J. Schwehr, D. Cherdack, R. Gran, GENIE implementation of IFIC valencia model for QE-like 2p2h neutrino–nucleus cross section. **1** (2016)
42. M. Betancourt et al., Direct measurement of nuclear dependence of charged current quasielasticlike neutrino interactions using MINER ν A. *Phys. Rev. Lett.* **119**(8), 082001 (2017)
43. P.A. Rodrigues et al., Identification of nuclear effects in neutrino-carbon interactions at low three-momentum transfer. *Phys. Rev. Lett.* **116**, 071802 (2016) (**Addendum: Phys. Rev. Lett.** **121**(20), 209902 (2018))
44. R. Gran et al., Antineutrino charged-current reactions on hydrocarbon with low momentum transfer. *Phys. Rev. Lett.* **120**(22), 221805 (2018)
45. C. Wilkinson, P. Rodrigues, S. Cartwright, L. Thompson, K. McFarland, Reanalysis of bubble chamber measurements of muon-neutrino induced single pion production. *Phys. Rev. D* **90**(11), 112017 (2014)
46. P. Rodrigues, C. Wilkinson, K. McFarland, Constraining the GENIE model of neutrino-induced single pion production using reanalyzed bubble chamber data. *Eur. Phys. J. C* **76**(8), 474 (2016)
47. M. Martini, N. Jachowicz, M. Ericson, V. Pandey, T. Van Cuyck, N. Van Dessel, Electron-neutrino scattering off nuclei from two different theoretical perspectives. *Phys. Rev. C* **94**(1), 015501 (2016)
48. J. Nieves, J.E. Sobczyk, In medium dispersion relation effects in nuclear inclusive reactions at intermediate and low energies. *Ann. Phys.* **383**, 455–496 (2017)
49. D. Ruterbories et al., Measurement of quasielastic-Like neutrino scattering at $\langle E_\nu \rangle \sim 3.5$ GeV on a hydrocarbon target. *Phys. Rev. D* **99**(1), 012004 (2019)
50. C.E. Patrick et al., Measurement of the muon antineutrino double-differential cross section for quasielasticlike scattering on hydrocarbon at $E_\nu \sim 3.5$ GeV. *Phys. Rev. D* **97**(5), 052002 (2018)
51. M.F. Carneiro et al., High-statistics measurement of neutrino quasielasticlike scattering at 6 GeV on a hydrocarbon target. *Phys. Rev. Lett.* **124**(12), 121801 (2020)
52. X.-G. Lu et al., Measurement of final-state correlations in neutrino muon-proton mesonless production on hydrocarbon at $\langle E_\nu \rangle = 3$ GeV. *Phys. Rev. Lett.* **121**(2), 022504 (2018)
53. A.P. Furmanski, J.T. Sobczyk, Neutrino energy reconstruction from one muon and one proton events. *Phys. Rev. C* **95**(6), 065501 (2017)
54. L. Harewood, R. Gran, Elastic hadron-nucleus scattering in neutrino–nucleus reactions and transverse kinematics measurements. **6** (2019)
55. T. Cai et al., Nucleon binding energy and transverse momentum imbalance in neutrino–nucleus reactions. *Phys. Rev. D* **101**(9), 092001 (2020)
56. A. Bodek, T. Cai, Removal energies and final state interaction in lepton nucleus scattering. *Eur. Phys. J. C* **79**(4), 293 (2019)
57. Y. Hayato, A neutrino interaction simulation program library NEUT. *Acta Phys. Pol. B* **40**, 2477–2489 (2009)
58. O. Buss, T. Gaitanos, K. Gallmeister, H. van Hees, M. Kaskulov, O. Lalakulich, A.B. Larionov, T. Leitner, J. Weil, U. Mosel, Transport-theoretical description of nuclear reactions. *Phys. Rep.* **512**, 1–124 (2012)
59. E.A. Paschos, J.-Y. Yu, M. Sakuda, Neutrino production of resonances. *Phys. Rev. D* **69**, 014013 (2004)
60. A. Bodek, T. Cai, Comparison of optical potential for nucleons and Δ resonances: in electron scattering from nuclear targets. *Eur. Phys. J. C* **80**(7), 655 (2020)
61. L.L. Salcedo, E. Oset, M.J. Vicente-Vacas, C. Garcia-Recio, Computer simulation of inclusive pion nuclear reactions. *Nucl. Phys. A* **484**, 557–592 (1988)
62. R. Merenyi, W.A. Mann, T. Kafka, W. Leeson, B. Saitta, J. Schneps, M. Derrick, B. Musgrave, Determination of pion intranuclear rescattering rates in muon-neutrino Ne versus muon–neutrino D interactions for the atmospheric neutrino flux. *Phys. Rev. D* **45**, 743–751 (1992)
63. E. Oset, L.L. Salcedo, Δ selfenergy in nuclear matter. *Nucl. Phys. A* **468**, 631–652 (1987)

64. O. Lalakulich, U. Mosel, Pion production in the Mini-BooNE experiment. *Phys. Rev. C* **87**(1), 014602 (2013)
65. E. Hernández, J. Nieves, M.J.V. Vacas, Single π production in neutrino–nucleus scattering. *Phys. Rev. D* **87**(11), 113009 (2013)
66. B. Eberly et al., Charged pion production in ν_μ interactions on hydrocarbon at $\langle E_\nu \rangle = 4.0$ GeV. *Phys. Rev. D* **92**(9), 092008 (2015)
67. C.L. McGivern et al., Cross sections for ν_μ and $\bar{\nu}_\mu$ induced pion production on hydrocarbon in the few-GeV region using MINERvA. *Phys. Rev. D* **94**(5), 052005 (2016)
68. O. Altinok et al., Measurement of ν_μ charged-current single π^0 production on hydrocarbon in the few-GeV region using MINERvA. *Phys. Rev. D* **96**(7), 072003 (2017)
69. D. Coplowe et al., Probing nuclear effects with neutrino-induced charged-current neutral pion production. *Phys. Rev. D* **102**(7), 072007 (2020)
70. T. Le et al., Single neutral pion production by charged-current $\bar{\nu}_\mu$ interactions on hydrocarbon at $\langle E_\nu \rangle = 3.6$ GeV. *Phys. Lett. B* **749**, 130–136 (2015)
71. T. Le et al., Measurement of $\bar{\nu}_\mu$ charged-current single π^- production on hydrocarbon in the few-GeV region using MINERvA. *Phys. Rev. D* **100**(5), 052008 (2019)
72. P. Stowell et al., Tuning the GENIE pion production model with MINERvA data. *Phys. Rev. D* **100**(7), 072005 (2019)
73. X.-G. Lu, J.T. Sobczyk, Identification of nuclear effects in neutrino and antineutrino interactions on nuclei using generalized final-state correlations. *Phys. Rev. C* **99**(5), 055504 (2019)
74. M.R. Alam, I.R. Simo, M.S. Athar, M.J.V. Vacas, Weak Kaon production off the nucleon. *Phys. Rev. D* **82**, 033001 (2010)
75. C.M. Marshall et al., Measurement of K^+ production in charged-current ν_μ interactions. *Phys. Rev. D* **94**(1), 012002 (2016)
76. C.M. Marshall et al., Measurement of neutral-current K^+ production by neutrinos using MINERvA. *Phys. Rev. Lett.* **119**(1), 011802 (2017)
77. A. Filkins et al., Double-differential inclusive charged-current ν_μ cross sections on hydrocarbon in MINERvA at $\langle E_\nu \rangle \sim 35$ GeV. *Phys. Rev. D* **101**(11), 112007 (2020)
78. B.G. Tice et al., Measurement of ratios of ν_μ charged-current cross sections on C, Fe, and Pb to CH at neutrino energies 2–20 GeV. *Phys. Rev. Lett.* **112**(23), 231801 (2014)
79. J. Mousseau et al., Measurement of partonic nuclear effects in deep-inelastic neutrino scattering using MINERvA. *Phys. Rev. D* **93**(7), 071101 (2016)
80. A. Bodek, U.-K. Yang, Axial and vector structure functions for electron- and neutrino–nucleon scattering cross sections at all Q^2 using effective leading order parton distribution functions. **11** (2010)
81. I.C. Cloet, W. Bentz, A.W. Thomas, EMC and polarized EMC effects in nuclei. *Phys. Lett. B* **642**, 210–217 (2006)
82. A. Higuera et al., Measurement of coherent production of π^\pm in neutrino and antineutrino beams on carbon from E_ν of 1.5 to 20 GeV. *Phys. Rev. Lett.* **113**(26), 261802 (2014)
83. A. Mislivec et al., Measurement of total and differential cross sections of neutrino and antineutrino coherent π^\pm production on carbon. *Phys. Rev. D* **97**(3), 032014 (2018)
84. C. Berger, L.M. Sehgal, PCAC and coherent pion production by low energy neutrinos. *Phys. Rev. D* **79**, 053003 (2009)
85. D. Rein, L.M. Sehgal, Coherent π^0 production in neutrino reactions. *Nucl. Phys. B* **223**, 29–44 (1983)
86. D. Rein, L.M. Sehgal, PCAC and the deficit of forward muons in π^+ production by neutrinos. *Phys. Lett. B* **657**, 207–209 (2007)
87. S.K. Singh, M.S. Athar, S. Ahmad, Nuclear effects in neutrino induced coherent pion production at K2K and MiniBooNE. *Phys. Rev. Lett.* **96**, 241801 (2006)
88. L. Alvarez-Ruso, L.S. Geng, S. Hirenzaki, M.J.V. Vacas, Coherent pion production in neutrino-nucleus collisions, in *23rd International Nuclear Physics Conference (INPC 2007)*, 9 (2007)
89. Z. Wang et al., First evidence of coherent K^+ meson production in neutrino-nucleus scattering. *Phys. Rev. Lett.* **117**(6), 061802 (2016)
90. D. Rein, Diffractive pion production in neutrino reactions. *Nucl. Phys. B* **278**, 61–77 (1986)
91. J. Wolcott et al., Evidence for neutral-current diffractive π^0 production from hydrogen in neutrino interactions on hydrocarbon. *Phys. Rev. Lett.* **117**(11), 111801 (2016)
92. R. Fine, B. Messerly, K.S. McFarland, Data Preservation at MINERvA (2020)
93. B. Messerly et al., An error analysis toolkit for binned counting experiments (2021)